# Hollow Fiber Membrane Contactors for Post-Combustion CO$_2$ Capture: A Scale-Up Study from Laboratory to Pilot Plant

E. Chabanon[1], E. Kimball[2]*, E. Favre[1], O. Lorain[3], E. Goetheer[2], D. Ferre[4],
A. Gomez[4] and P. Broutin[4]

1 Laboratoire Réactions et Génie des Procédés, LRGP (UPR CNRS 3349), 1 rue Grandville, 54000 Nancy - France
2 TNO, Leeghwaterstraat 46, 2628 CA Delft - The Netherlands
3 Polymem, impasse du Palayré, 31100 Toulouse - France
4 IFP Energies nouvelles-Lyon, Rond-point de l'échangeur de Solaize, BP 3, 69360 Solaize - France
e-mail : elodie.chabanon@ensic.inpl-nancy.fr - erin.kimball@tno.nl - eric.favre@ensic.inpl-nancy.fr - o.lorain@polymem.fr - earl.goetheer@tno.nl
daniel.ferre@ifpen.fr - adrien.gomez@ifpen.fr - paul.broutin@ifpen.fr

\* Corresponding author

**Résumé** — **Captage postcombustion du CO$_2$ par des contacteurs membranaires de fibres creuses : de l'échelle laboratoire à l'échelle pilote industriel** — Depuis des décennies, les contacteurs membranaires sont proposés pour intensifier les procédés de transfert de matière. Le captage post-combustion du CO$_2$ par absorption dans un solvant chimique est actuellement l'un des sujets le plus intensivement examiné. Un grand nombre d'études ont déjà été reportées dans la littérature, malheureusement, elles ne concernent pratiquement que des expériences menées à l'échelle laboratoire sur de petits modules. Étant donné les débits de fumées qui doivent être traités dans une application industrielle du captage du CO$_2$, une étude consistante à plus grande échelle est nécessaire à l'obtention d'un design rigoureux du procédé. Dans cette étude, les possibilités et les limites de l'échelle laboratoire et de l'échelle pilote industrielle ont été évaluées et seront discutées. Les expériences (absorption du CO$_2$ d'un mélange gazeux par une solution aqueuse de MEA à 30 % mass.) ont été menées à la fois sur un mini-module à l'échelle laboratoire et sur un module de taille industrielle (10 m$^2$), tous deux constitués de fibres PTFE. L'approche des résistances en série a ensuite été utilisée pour simuler les résultats. Un seul paramètre ajustable est utilisé : le coefficient de transfert de matière dans la membrane ($k_m$) qui joue logiquement un rôle clé. Les difficultés et les incertitudes des calculs liées au changement d'échelle, plus particulièrement sur la valeur de $k_m$, sont présentées et discutées.

*Abstract* — *Hollow Fiber Membrane Contactors for Post-Combustion CO$_2$ Capture: A Scale-Up Study from Laboratory to Pilot Plant* — *Membrane contactors have been proposed for decades as a way to achieve intensified mass transfer processes. Post-combustion CO$_2$ capture by absorption into a chemical solvent is one of the currently most intensively investigated topics in this area. Numerous studies have already been reported, unfortunately almost systematically on small, laboratory scale, modules. Given the level of flue gas flow rates which have to be treated for carbon capture applications, a consistent scale-up methodology is obviously needed for a rigorous engineering design. In this study, the possibilities and limitations of scale-up strategies for membrane contactors have been explored and will be discussed. Experiments (CO$_2$ absorption from a gas mixture in a 30%wt MEA aqueous solution) have been performed both on mini-modules and at pilot-scale (10 m$^2$ membrane contactor module) based on*

*PTFE hollow fibers. The results have been modeled utilizing a resistance in series approach. The only adjustable parameter is in fitting the simulations to experimental data is the membrane mass transfer coefficient ($k_m$), which logically plays a key role. The difficulties and uncertainties associated with scale-up computations from lab scale to pilot-scale modules, with a particular emphasis on the $k_m$ value, are presented and critically discussed.*

## NOMENCLATURE

| | |
|---|---|
| $c$ | Concentration (mol.m$^{-3}$) |
| $C_p$ | Heat capacity (J.K$^{-1}$.kg$^{-1}$) |
| $D$ | Diffusion coefficient (m$^2$.s$^{-1}$) |
| $H$ | Enthalpy of reaction (J.mol$^{-1}$) |
| $K_i$ | Equilibrium constant of reaction $i$ (-) |
| $k_{app}$ | Apparent constant of equilibrium (-) |
| $r$ | Radial coordinate (m) |
| $r_i$ | Inner fiber radius (m) |
| $r_o$ | Outer fiber radius (m) |
| $r_g$ | Inner shell radius (m) |
| $R$ | Reaction rate (mol.m$^{-3}$.s$^{-1}$) |
| $T$ | Temperature (K) |
| $v$ | Interstitial velocity (m.s$^{-1}$) |
| $z$ | Axial coordinate (m) |
| $\varphi$ | Packing ratio (-) |
| $\kappa$ | Thermal conductivity (W.m$^{-1}$.K$^{-1}$) |
| $\rho$ | Density (kg.m$^{-3}$) |

## ABBREVIATIONS

| | |
|---|---|
| MEA | MonoEthanolAmine |
| PP | PolyPropylene |
| PTFE | PolyTetraFluoroEthylene |
| PVDF | PolyVinyliDeneFluoride |

## INTRODUCTION

The rise of greenhouse gases in the atmosphere is commonly accepted to be caused by anthropological emissions and could be responsible for global climate change. This results in serious damage to the environment in the forms of retreating glaciers, rising sea-level and increasing storm intensity [1]. It is established that $CO_2$ is one of the most important greenhouse gases due to the immense volumes and increasing rates at which it is emitted to the atmosphere. This is mostly due to the constantly growing demand for energy, an industry which emits around 30 billion tons of $CO_2$ each year worldwide [2].

In January 2007, the European Commission recommended to the member states to cut their collective greenhouse gas emissions by 20% from the 1990 levels by 2020 [3]. Carbon Capture and Storage (CCS) is thus considered to be an essential component in the strategy to meet the ambitious emissions reduction goals and must be applied to both new power plants and as a retrofit to existing plants [4].

For existing power plants, the $CO_2$ must be removed after the fuel combustion. This results in a dilute stream of $CO_2$, about 14% vol. [5], in nitrogen for a coal power plant. The conditions of the flue gas are mild at atmospheric pressure and about 40°C, but the flow rates are immense, around 600 m$^3$/s for an 800 MW coal fired power plant. The typical systems required to separate the $CO_2$ at low concentrations involve contacting the flue gas with a solvent, which reacts chemically with the $CO_2$ and is later regenerated by either a pressure or temperature swing [6]. In order to achieve a capture rate of about 90%, huge contact surface areas are required, about 700 000 m$^2$ for the example above.

The conventional design for providing such high contact surface areas is with one or more large towers filled with a structured packing material. The flue gas is introduced at the bottom of the column and flows counter-currently to the solvent liquid introduced at the top. The size of these columns, at least 10 m in diameter and at least four times as high, makes them both expensive and difficult to install when space is limited.

As an alternative, the utilization of membrane contactors could be a promising process for $CO_2$ capture [7, 8]. With Hollow Fiber Membrane Modules (HFMM), the liquid solvent flows inside the membrane fiber tubes (lumen side) while the $CO_2$-rich gas flows around the outside of the fibers (shell side) [9-11] or *vice versa* [12-14]. The gas is transported through the (ideally) liquid-free pores of the membrane to come into contact with the liquid where it reacts with MEA. Thousands of fibers are bundled tightly together within each module, with several modules in parallel to achieve the desired capture rate of $CO_2$. In comparison to packed columns, HFMM avoid several operational problems including flooding, channeling, foaming and entrainment. Gas absorption membrane systems offer further advantages, such as independent control of the gas and liquid flows, linear scale-up [15] and a significant size reduction, with a specific surface area (m$^2$.m$^{-3}$) between two and ten times greater than with packed columns [16].

The focus of much of the work investigating the operation of HFMM has been on modeling and predicting the mass transfer characteristics of the $CO_2$ across the membrane, usually with limited experimental data for comparison. The earlier models solve the mass balances in two dimensions in order to compare the radial and axial concentration profiles at different gas flow rates, liquid flow rates and temperatures [17, 18]

*E. Chabanon* et al. / *Hollow Fiber Membrane Contactors for Post-Combustion CO$_2$ Capture:*
*A Scale-Up Study from Laboratory to Pilot Plant*

3

and also with varying solvents [19, 20]. More recent work has looked at the transient behavior of gas absorption into a liquid [21], predictions using computational fluid dynamics [22] and effects of the wetting behavior of the membrane [23-25]. In addition to CO$_2$ capture, HFMM are also being investigated for H$_2$S absorption, by experimentally looking at the effect of different solvent concentrations [26] and by both experimentally and theoretically looking at the effects of module design and flow rates [27].

The work discussed here has extended the traditional approach to investigate the implications of scale-up for these systems. A lab-scale membrane module system was constructed in order to validate a mass transfer model similar to those discussed above. The validated model was then used for simulation of a full scale system. The results of the full scale simulation were then compared with experimental data from an industrial pilot-scale membrane system utilizing the same materials as those for the lab-scale. In general, this study intends to evaluate and discuss the possibilities and limitations of scale-up strategies for membrane contactors through these two case studies.

# 1 MATERIAL AND METHODS

## 1.1 Membrane Characterization

In the first step, a literature review combined with the partners' experience in membrane testing [28] and contactor development [29] showed that even though a very large number of studies on CO$_2$ absorption in membrane contactors have been reported [9-14, 30-33], several key issues remain largely unexplored. Among them, the stability in time of the material which is used for the membrane in the contactor appears to be of primary importance but poorly documented. Most studies report lab-scale experiments only on a short term basis (*i.e.* on an hours or days scale [34-36]). Consequently, the following priority targets are defined, in order to select the most appropriate materials for module preparation:

– a series of 10 different commercially available flat sheet membrane materials, based on 4 different polymer types — polypropylene (PP), polyvinylidenefluoride (PVDF), polytetrafluoroethylene (PTFE) and nylon — are selected for experimental tests;

– native membrane material properties, such as gas permeability and contact angle, are determined;

– the evolution of the previous properties when the samples are put in contact with a 30%wt monoethanolamine (MEA) aqueous solution are investigated on a long time basis (*i.e.* up to 2 months exposure) at temperatures of 293.15, 313.15 and 353.15 K.

In parallel, compatibility tests of the solvent solution with different glue and casing candidate materials were also performed. The results of the aging tests (evolution of contact angle and gas permeability with time) unambiguously and consistently show that:

– PTFE (5 different samples) demonstrates a remarkable stability with time in terms of gas permeability and stability of the non wetting properties, both at 313.15 and 353.15 K;

– PP (1 sample) and PVDF (3 different samples) present a fair to reasonable stability of gas permeability and contact angle with time at 313.15 K, but degrade significantly at 353.15 K;

– nylon does not show a good stability in MEA solutions, both at 313.15 and 353.15 K.

From the conclusions of this preliminary work, PTFE is selected as the most appropriate membrane material for the membrane contactor designs. A tailor made PTFE hollow fiber has been provided by Polymem and samples are characterized more fully.

Several studies are done to characterize the porosity of the fibers. The first is the Hg method (mercury intrusion technique) as it is the usual method for catalysts. The main result is that the internal structure of the sample is mainly macro-porous. The pores are comprised of sizes between 1 and 10 µm, with a mean value of 5-6 µm and a mean porosity of 0.28 mL/g. The second study is an X-rays analysis done at the European Synchrotron Radiation Facility in Grenoble (France). A typical reconstructed 3D view is shown in Figure 1. Globally, the pores form interconnected compartments, flattened in the direction of the length of the fiber (anisotropic texture). From the zoom-ins in the right part of the figure, one can see that the pores are very well connected in the axial direction and that the superficial porosity is very high, both on the inner and outer sides of the fibbers. The flattened aspect of the pores is not adequate for the usual definition of the pore sizes which supposes an isotropic distribution. In good accordance with the Hg
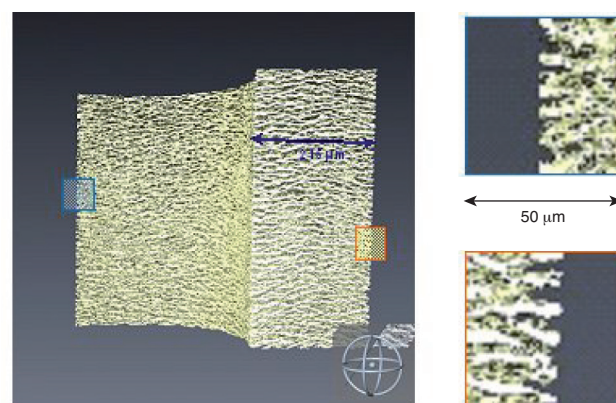


Figure 1

Synchrotron analysis of the PTFE hollow fiber tested at lab and pilot-scale in this study (image obtained at the European Synchrotron Radiation Facility).

analysis, it is again found that 5 μm is the typical dimension of the pore in the radial direction, but the straight pass length is quite scattered with an apparent mean value of about 30 μm and some passes reaching almost 100 μm.

## 1.2 Experimental Set-Up

### 1.2.1 Lab-Scale

The lab-scale membrane contactor is constructed utilizing the chosen PTFE fibers for the membrane polymer, as described above. A photo and diagram of the module setup are shown in Figure 2 and the module's geometrical properties are summarized in Table 1.

Mixtures of $CO_2$ and $N_2$ are prepared using two mass flow controllers and fed to the shell side of the membrane fibers. An aqueous 30%wt MEA solution is prepared by dilution of high purity MEA in distilled water. The liquid phase flows in the lumen side, counter-currently to the gas phase. The liquid flow rate is controlled by a high precision pump and the pressure is regulated by a valve placed at the liquid outlet.

During the experiments, the pressure and temperature are both at ambient conditions (1 bar and ~ 20°C). The inlet $CO_2$ volume fraction is 14-15%vol. with total gas flow rates of $25 \times 10^{-3}$ – 6.00 L.min$^{-1}$. Fresh 30%wt MEA solution is used in each case with flow rates of $(10 \times 10^{-3})$ - $(50 \times 10^{-3})$ L.min$^{-1}$. An Infra-Red (IR) analyzer is used to measure the $CO_2$ volume fraction in the gas at both the inlet and outlet of the module. A bubble meter is used to measure the gas flow rate at the inlet and at the outlet of the module. Particular attention is paid to achieve steady-state conditions for each measurement, reflected by a constant $CO_2$ volume fraction at the outlet.

TABLE 1

Details of the lab-scale HFMM

| | | |
|---|---|---|
| | Inner diameter (m) | $1.24 \times 10^{-2}$ |
| | Effective length (m) | 0.30 |
| | Length (m) | 0.35 |
| Module | Number of fibers (-) | 119 |
| | Packing ratio (-) | 0.59 |
| | Specific interfacial area (m$^2$.m$^{-3}$) | 1 331 |
| | Inner diameter (m) | $4.30 \times 10^{-4}$ |
| Fiber | Outer diameter (m) | $8.70 \times 10^{-4}$ |
| | Porosity (-) | 0.336 |

### 1.2.2 Industrial Pilot-Scale

The pilot-scale module is constructed to be more than two orders of magnitude larger than the mini-module, both by increasing the length of the module and the number of fibers. Approximately equal specific interfacial areas (m$^2$.m$^{-3}$) and liquid phase Reynolds numbers of the same order of magnitude ensured dimensional similarity between the mini-module and pilot-scale. Due to the large number of fibers required for the industrial membrane module, 8 521, the bundle is supported by a plastic grid which is rolled into a spiral inside the fiber bundle. The grid is needed to support the fibers during the implementation of the resin sealing to make the bundle. An X-rays analysis showing the cross-section of the bundle and the plastic grid are given in Figures 3a and 3b, respectively. The presence of the grid does not appear to disrupt the distribution of the fibers over the length of the bundle to a large degree; however, the dark spaces in Figure 3a indicate



Figure 2

Photo and diagram of the lab-scale set-up for the $CO_2$ absorption experiments with mini HFMM.
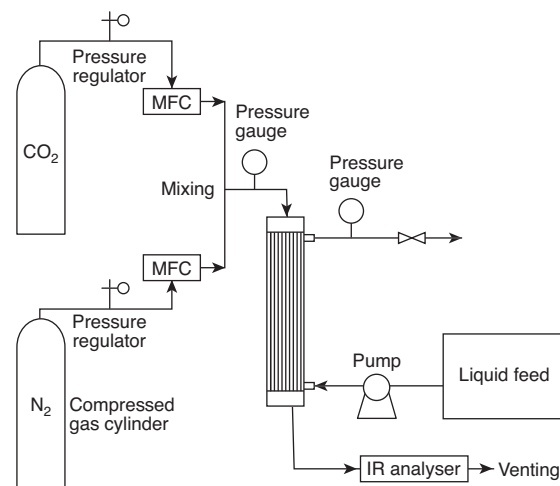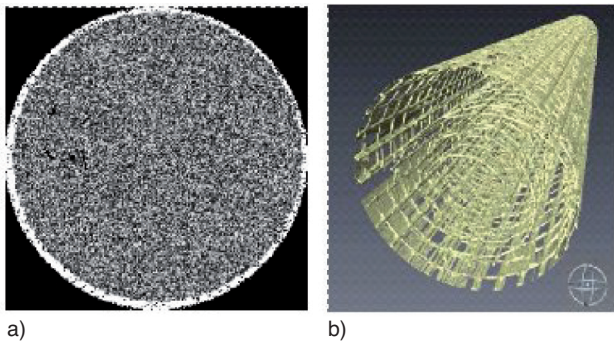
Figure 3

X-rays analysis of the pilot-scale HFMM. a) Fiber bundle cross-section. b) Plastic grid wound inside the fiber bundle.

TABLE 2

Details of pilot-scale HFMM

| | | |
|---|---|---|
| | Inner diameter (m) | 0.105 |
| | Length (m) | 0.88 |
| Module | Effective length (m) | 1 |
| | Number of fibers (-) | 8 521 |
| | Packing ratio (-) | 0.648 |
| | Specific interfacial area ($m^2.m^{-3}$) | 1 329 |
| | Inner diameter (m) | $4.30 \times 10^{-4}$ |
| Fiber | Outer diameter (m) | $8.70 \times 10^{-4}$ |
| | Porosity (-) | 0.336 |

some void spaces where preferential channeling of the gas flow may occur.

The final parameters of the industrial module are given in Table 2.

A diagram of the setup of the entire system is shown in Figure 4. The liquid flows axially from bottom to top and an inline transparent section (2) follows the liquid outlet, allowing for observation of possible bubbles. Keeping the counter-current mode, the gas, therefore, flows from top to bottom and an inline transparent filter (1) is installed at the gas outlet to catch any liquid that could percolate through the membrane.

The absorption of $CO_2$ is tested using a $CO_2/N_2$ mixture. The flow rate of $N_2$ and the concentration of the $CO_2$ are kept constant during each test-run using control valves. The liquid circuit is a closed loop including a 600 L storage tank open to the atmosphere. The MEA solvent reaches the module through a pump-controlled valve-flow meter system and flows back to the tank by gravity. A bend and a valve placed at the liquid outlet of the module are used to maintain a constant pressure in the liquid phase. This facility is used for the
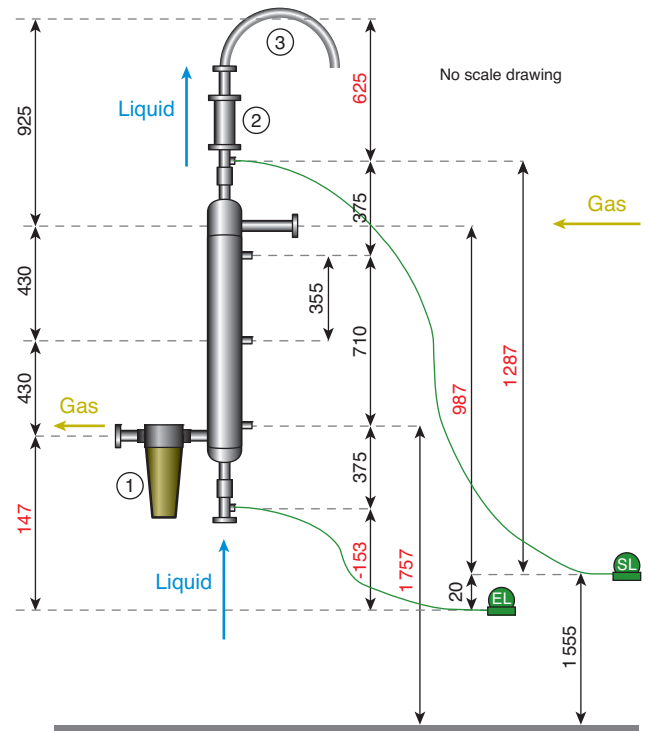


Figure 4

Diagram of the pilot-scale HFMM setup.

highest gas flow rates to prevent the gas from passing through the hollow membrane fibers.

The pressure drops of the gas phase and the liquid phase are measured by four relative-to-atmosphere pressure transducers connected to the inlet and the outlet of each phase. For both types of modules (mini and pilot), the pressure of the gas phase had to be monitored so as not to be high enough to cause bubbling into the liquid phase.

Two small lines from the gas inlet and outlet running down to the control room and made of capillary tubes are connected to IR sensors to measure the $CO_2$ concentration. Finally, the liquid inlet and outlet are equipped with bleed valves which allow for sampling of the liquid phase in order to measure the mass fraction of MEA and the $CO_2$ loading of the liquid phase over time.

As with the lab-scale experiments, each measurement is taken when steady state conditions are reached.

## 2 THEORETICAL STUDIES

In this study, a 2D mathematical model is developed for the transport of $CO_2$ from the gas phase into an aqueous MEA solution within an HFMM. This model is developed for a single hollow fiber, as shown in Figure 5. The setup of the
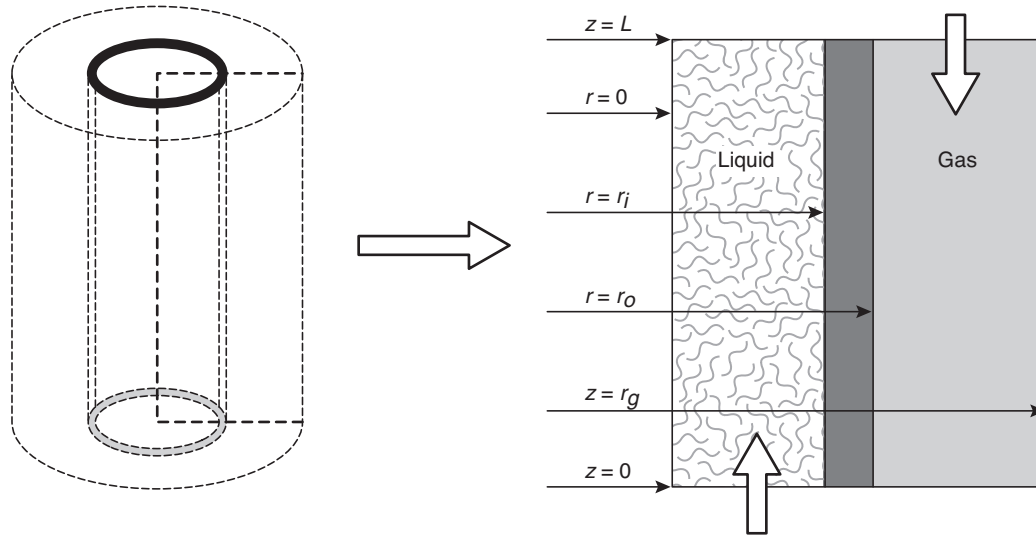
Figure 5

Schematic diagram of the membrane fiber simulated in the 2D model.

model is similar to those most commonly found in the literature [17, 19, 22-24, 26, 37] with the three layers — shell, membrane and lumen — treated separately according to a resistance-in-series approach.

The differential mass and energy balances in the axial and radial directions over a single fiber are considered:

– shell side (gas phase): diffusion and convection, no reaction ($i = CO_2, N_2$):

$$D_i^{shell}\left[\frac{\partial^2 c_i^{shell}}{\partial r^2} + \frac{1}{r}\frac{\partial c_i^{shell}}{\partial r}\right] - v_z^{shell}\frac{\partial c_i^{shell}}{\partial z} = 0 \qquad (1)$$

$$\kappa^{shell}\left[\frac{\partial^2 T^{shell}}{\partial r^2} + \frac{1}{r}\frac{\partial T^{shell}}{\partial r}\right] - \rho\, C_p v_z^{shell}\frac{\partial T^{shell}}{\partial z} = 0 \qquad (2)$$

– membrane: diffusion only ($i = CO_2, N_2$):

$$D_i^{mem}\left[\frac{\partial^2 c_i^{mem}}{\partial r^2} + \frac{1}{r}\frac{\partial c_i^{mem}}{\partial r}\right] = 0 \qquad (3)$$

$$\kappa^{mem}\left[\frac{\partial^2 T^{mem}}{\partial r^2} + \frac{1}{r}\frac{\partial T^{mem}}{\partial r}\right] = 0 \qquad (4)$$

– lumen side (liquid phase): diffusion, convection and reaction ($i = CO_2, H_2O, MEA$):

$$D_i^{lumen}\left[\frac{\partial^2 c_i^{lumen}}{\partial r^2} + \frac{1}{r}\frac{\partial c_i^{lumen}}{\partial r}\right] - v_z^{lumen}\frac{\partial c_i^{lumen}}{\partial z} + R_i = 0 \qquad (5)$$

$$\kappa^{lumen}\left[\frac{\partial^2 T^{lumen}}{\partial r^2} + \frac{1}{r}\frac{\partial T^{lumen}}{\partial r}\right] - \rho\, C_p v_z^{lumen}\frac{\partial T^{lumen}}{\partial z} + R_i\sum H_i^{lumen} = 0 \;(6)$$

In the equations above, $D_i$ is the diffusion coefficient of the species $i$ in each layer ($m^2.s^{-1}$), $c_i$ is the concentration of the species $i$ in each layer ($mol.m^{-3}$), $v$ is the interstitial velocity

defined as below ($m.s^{-1}$), $R$ is the reaction rate ($mol.m^{-3}.s^{-1}$), $r$ is the radial coordinate (m), $z$ is the axial coordinate (m), $T$ is the temperature (K), $\rho$ is the density ($kg.m^{-3}$), $\kappa$ is the thermal conductivity of each layer ($W.m^{-1}.K^{-1}$), $H_i$ is the enthalpy of reaction of the species $i$ with the MEA ($J.mol^{-1}$) and $C_p$ is the thermal capacity ($J.K^{-1}.kg^{-1}$).

The three layers considered are connected by the following interface relations and boundary conditions:

– axial direction (assuming counter-current flow pattern):

$$z = 0,\; T^{lumen} = T_{in}^{lumen},\;\; c_i^{lumen} = 0 \text{ for } i = CO_2,$$
$$c_i^{lumen} = c_{i,in}^{lumen} \text{ for } i = MEA, H_2O$$

$$z = L,\; T^{shell} = T_{in}^{shell},\;\; c_i^{shell} = c_{i,in}^{shell} \text{ for } i = CO_2,$$
$$c_i^{shell} = 0 \text{ for } i = MEA, H_2O$$

– radial direction:

$$r = 0,\; \frac{\partial T^{lumen}}{\partial r} = 0,\; \frac{\partial c_i^{lumen}}{\partial r} = 0 \quad \text{for } i = \text{all species}$$

$$r = r_i,\; T^{lumen} = T^{mem},\; \frac{\partial c_i^{lumen}}{\partial r} = 0 \quad \text{for } i = \text{amine species},$$
$$c_i^{lumen} = m\, c_i^{mem} \text{ for } i = CO_2, H_2O$$

$$r = r_o,\; T^{mem} = T^{shell},\; c_i^{mem} = c_i^{shell} \text{ for } i = CO_2, H_2O,$$
$$c_i^{mem} = 0 \text{ for } i = MEA$$

$$r = r_g,\; \frac{\partial T^{shell}}{\partial r} = 0,\; \frac{\partial c_i^{shell}}{\partial r} = 0 \quad \text{for } i = CO_2, H_2O,$$
$$c_i^{shell} = 0 \text{ for } i = MEA$$

E. Chabanon et al. / Hollow Fiber Membrane Contactors for Post-Combustion $CO_2$ Capture: A Scale-Up Study from Laboratory to Pilot Plant
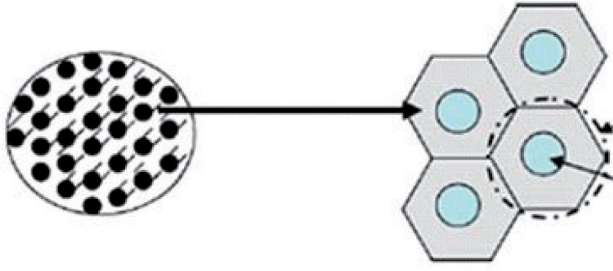
7



Figure 6

Membrane module cross section and approximation of the gas shell surrounding the fibers according to the Happel's free surface model [26].

The implementation is based on the method of lines and executed in Matlab. The specifications used are: gas flow on the shell side of the fibers, liquid flow on the lumen side and counter-current flows. The key assumptions are as follows:

– negligible axial diffusion (in the gas and liquid phases);
– amine compounds and water only present in the liquid phase (no evaporation);
– no wetting of the membrane pores;
– uniform fiber shapes and packing.

The flow of the liquid on the tube side of the membrane is assumed to be fully-developed laminar parabolic flow, as supported by low Reynolds numbers (on the order of 100) for the conditions tested in the experiments:

$$c_i^{lumen} = 2\langle v \rangle \left[ 1 - \left( \frac{r_i}{r} \right)^2 \right] \tag{7}$$

where $\langle v \rangle$ is the average velocity (m.s$^{-1}$) and $r_i$ is the inner radius of the fiber (m).

It should be noted that non-idealities in the fiber shapes (bends, inconsistent diameters, etc.) introduce mixing in the lumen side of the fibers, but this is not considered in the model.

The flow of gas on the shell side of the membrane is modeled using Happel's free surface model [38] *(Fig. 6)*:

$$v_z^{shell} = 2\langle v \rangle \left[ 1 - \left( \frac{r_o}{r_g} \right)^2 \right] \left[ \frac{\left( \frac{r}{r_g} \right)^2 - \left( \frac{r_o}{r_g} \right)^2 + 2\ln\left( \frac{r_o}{r} \right)}{3 + \left( \frac{r_o}{r_g} \right)^4 - 4\left( \frac{r_o}{r_g} \right)^2 + 4\ln\left( \frac{r_o}{r_g} \right)} \right] \tag{8}$$

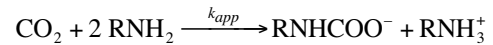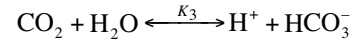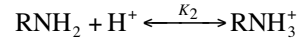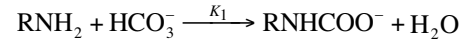$$r_g = r_o \sqrt{\frac{1}{1 - \varphi}} \tag{9}$$

where $r_o$ is the outer radius of the fiber, $r_g$ is the gas shell radius (m) and $\varphi$ is the packing ratio of the module.

This equation assumes uniform laminar flow around each of the fibers. It is known that the construction of HFMM

may result in a highly non-uniform distribution of the fibers within the module. Therefore, the Happel's free surface model is mostly used to calculate the effective diameter of the gas shell around each fiber and the non-uniformity of the gas flow is accounted for in the adjustment of the mass transfer across the membrane.

For the membrane, the only mechanism of mass transfer considered is diffusion.

A simplified mechanism for the kinetics is used to formulate the overall reaction rate expression, as given below:

$$RNH_2 + HCO_3^- \xrightarrow{K_1} RNHCOO^- + H_2O$$

$$RNH_2 + H^+ \xleftarrow{K_2} RNH_3^+$$

$$CO_2 + H_2O \xleftarrow{K_3} H^+ + HCO_3^-$$

$$\overline{CO_2 + 2\,RNH_2 \xrightarrow{k_{app}} RNHCOO^- + RNH_3^+}$$

The full reaction mechanism for $CO_2$-MEA-$H_2O$ systems is more complex than that given here, involving several acid-base reactions [39]. These acid-base reactions are not considered here as they allow for the calculation of the concentrations of $H^+$ ions and water. In this case, experimental data are available for the equilibrium pH *versus* temperature and $CO_2$ partial pressure, allowing for direct calculation of the concentration of $H^+$ ions based on the $CO_2$ concentration, assuming a fast reaction time of the acid-base reactions relative to the reactions with $CO_2$ and amine species. Also, the concentration of $H_2O$ is assumed to be constant as there is a large excess of water (70%wt) in the solution.

The expressions for the equilibrium constants for the specific reactions above are obtained from literature, including forward and backward rate constants, and are dependent on temperature. Conservation of mass for the amine species (RNH group) is also used in deriving the final rate expression:

$$R_{CO_2} = k_3 \left[ CO_2 \right] - \frac{k_{-3} K_1 [H^+][RNHCOO^-]}{[RNH_2]} \tag{10}$$

The concentrations of $CO_2$, $RNHCOO^-$ (carbamate) and $RNH_2$ (MEA) are calculated at each point of the model grid discretization by solving the corresponding model differential equations.

## 3 RESULTS AND DISCUSSION

### 3.1 Results from Lab-Scale Setup

The membrane mass transfer coefficient, $k_m$ (m.s$^{-1}$), is defined by:

$$k_m = \frac{D^{mem}\varepsilon}{\tau\delta}$$

where $D^{mem}$ is the membrane diffusion coefficient ($m^2.s^{-1}$), $\varepsilon$ is the membrane porosity (-), $\tau$ is the membrane tortuosity (-) and $\delta$ is the membrane thickness (m).

By adjusting the value of $k_m$ for $CO_2$, the experimental results from the lab-scale module fit very well with the model predictions. The value of $k_m$ is fit to the data by hand using one liquid flow rate of $50 \times 10^{-3}$ L.min$^{-1}$ and an intermediate gas flow rate of 3.00 L.min$^{-1}$. The value is adjusted in the model until the calculated $CO_2$ percentage at the outlet is about equal to the experimental value. The best fit is found using a value of:

$$k_m = 2.58 \times 10^{-4} \text{ m.s}^{-1}$$

The results of the simulations from the model compared to the experimental data are shown in Figure 7, given in terms of both the volume fraction of $CO_2$ at the outlet of the gas phase *(Fig. 7a)* and as the capture rate of $CO_2$ *(Fig. 7b)*, both *versus* the gas flow rate at the inlet of the shell side. All of the points shown are with an inlet $CO_2$ volume fraction of approximately 15%, fresh 30% wt MEA and an inlet solvent flow rate of either $10 \times 10^{-3}$ or $50 \times 10^{-3}$ L.min$^{-1}$. The results for the higher liquid flow rate, $Q_l = 50 \times 10^{-3}$ L.min$^{-1}$, fit extremely well over the range of gas flow rates, from $50 \times 10^{-3}$ to 6.00 L.min$^{-1}$, where the data also follows a smooth trend. At the lower liquid flow rate, $Q_l = 10 \times 10^{-3}$ L.min$^{-1}$, there are larger differences between the experimental and model results but more fluctuations in the data are also observed.

With the close fit between the model and experimental results, the model is considered to be validated and able to describe the 2D mass transfer of $CO_2$ across the membrane and its absorption into the solvent.

## 3.2 Results from Pilot-Scale Setup

Several experiments with varying liquid and gas flow rates were conducted with the industrial pilot-scale HFMM. The results considered here are for a range of liquid flow rates of 0.50-3.33 L.min$^{-1}$ and gas flow rates of 5-30 L.min$^{-1}$. The MEA is recirculated and so is already partially loaded with $CO_2$, which is also measured at the start of each experiment. The inlet volume fraction of $CO_2$ in the $N_2$ is kept approximately constant at about 15%. The experimental results are then compared with simulation results from the 2D mass transfer model.

Following the validation of the 2D model with the data from the lab-scale module, the parameters of the model describing the module design and MEA conditions are adjusted to simulate the pilot-scale module. The fibers in both modules are made from the same material, allowing for the membrane mass transfer coefficient determined from the fit with the lab-scale module experimental data to also be used in the simulations of the larger module. However, the results of the pilot-scale module simulations using the previously determined $k_m$ value show a significant over-prediction of the $CO_2$ capture for all of the gas and liquid flow rates, indicated by very low values for the $CO_2$ volume fraction at the outlet of the gas phase, as shown in Figure 8.

In order to have the model fit the experimental data at an intermediate gas flow rate of 10 L.min$^{-1}$, the membrane mass transfer coefficient is adjusted to:
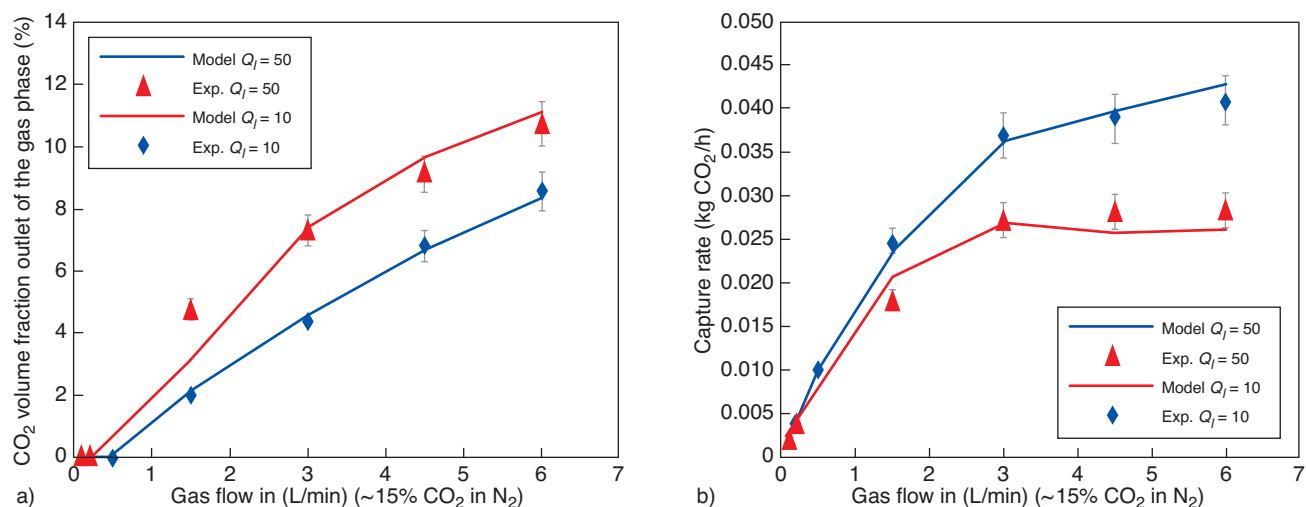
$$k_m = 5.31 \times 10^{-5} \text{ m.s}^{-1}$$



Figure 7

Comparison of simulation results and experimental data for the mini HFMM for gas inlet flow rates of $50 \times 10^{-3}$ to 6.00 L.min$^{-1}$ and two liquid flow rates, $Q_l = 10 \times 10^{-3}$ and $50 \times 10^{-3}$ L.min$^{-1}$. a) Results for $CO_2$ volume fraction at the outlet of the shell side. b) Results for calculation of the capture rate (kg $CO_2$ captured per hour).

E. Chabanon et al. / Hollow Fiber Membrane Contactors for Post-Combustion $CO_2$ Capture:
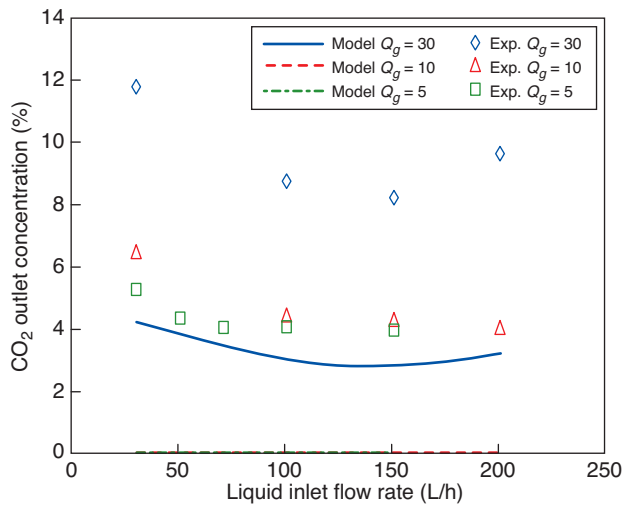A Scale-Up Study from Laboratory to Pilot Plant

9

Figure 8

Comparison of simulation results and experimental data for the pilot-scale module utilizing the $k_m$ value from the fit with the mini-module data. Values are given as $CO_2$ volume fraction at the outlet of the gas phase for liquid inlet flow rates of 0.50-3.33 L.min$^{-1}$ and gas inlet flow rates of 5, 10 or 30 L.min$^{-1}$. The inlet volume fraction of $CO_2$ is about 15% in every case and the accuracy of the $CO_2$ detector is ± 0.01%.
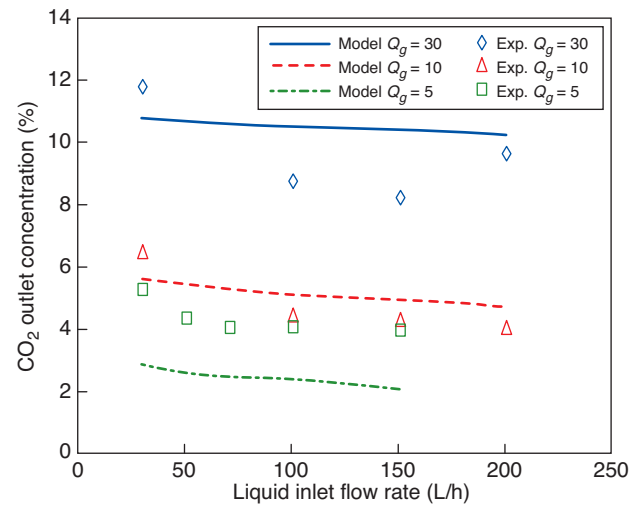


Figure 9

Comparison of simulation results and experimental data for the pilot-scale module utilizing a $k_m$ value of $5.31 \times 10^{-5}$ m.s$^{-1}$. Values are given as $CO_2$ volume fraction at the outlet of the shell side for liquid inlet flow rates of 0.50-3.33 L.min$^{-1}$ and gas inlet flow rates of 5, 10 or 30 L.min$^{-1}$. The inlet fraction of $CO_2$ is about 15% vol. in every case and the accuracy of the $CO_2$ detector is ± 0.01% (same experimental data as in Fig. 8).

and gives good results over the range of liquid flow rates, as shown in Figure 9 (red markers). However, for the lower gas flow rate of 5 L.min$^{-1}$ (green markers), the simulations show a lower prediction of the $CO_2$ volume fraction at the outlet and at a higher gas flow rate of 30 L.min$^{-1}$ (blue markers), the prediction of the percent $CO_2$ is higher than what is observed experimentally. The effects of the different parameters on the results are investigated separately but the simulation results cannot be made to fit well with all of the data sets with one set of parameter values. This indicates that the non-idealities in the larger pilot-scale system are much more significant than with the lab-scale module, as logically expected. The 2D mass transfer model with the stated assumptions cannot account for the different phenomena occurring in the pilot-scale module.

## 3.3 Comparison between Lab-Scale and Pilot-Scale

The significant differences in the results between the lab- and pilot-scale modules show the difficulties in predicting the performance of larger scale systems with simple models. It is important to stress that the modeling approach tested in this study corresponds to the basic 2D equations classically proposed in membrane contactor studies. The comparison performed here shows that significant improvements need to be incorporated into the 2D mass transfer model before the operation of a full scale module will be acceptably simulated

over a wide range of conditions. When simulating the pilot-scale module, the over-prediction of the $CO_2$ capture may be due to errors in the mass transfer parameters, kinetics or assumptions of uniformity. Given that the $k_m$ value is set by fitting the data from the small lab-scale module, it is thought that the maldistribution of gas flow around the fibers of the pilot-scale module, especially with the mesh grid that is incorporated into the fiber bundle, is the most significant source of error. This would effectively make the resistance of the gas flow through the membrane appear higher. The mass transfer resistance of the gas flow close to the fibers is still relatively low, but not all of the gas flows in the shell of a fiber, as defined by Happel's free surface model. The resistance to mass transfer through the membrane for some fraction of the $CO_2$ in the gas phase would then be essentially infinite.

Another source of error that would be much more significant with the pilot-scale module than with the lab-scale module is the effect of the temperature rise due to the heat of the absorption reaction. The model assumed no evaporation of water from the lumen of the fibers to the gas phase. However, evaporation may be a significant factor, given that the gas is dry at the inlet and the simulations predicted about a 10°C temperature rise over the length of the fiber, for the pilot-scale module. This is supported by the fact that a large amount (approximately 10 L but not precisely measured) of condensed water is present in the outlet of the experimental pilot-scale system between tests. In contrast, the predicted

temperature rise for the much smaller lab-scale module is less than 1°C and no water condensation in the experimental setup is reported. The effect that the water evaporation can have on the $CO_2$ capture performance is to decrease the capture ratio. As water evaporates into the gas phase, the partial pressure of $CO_2$ in the gas phase decreases; this in turn decreases the driving force for $CO_2$ transport through the membrane and into the absorption liquid, thus resulting in a lower $CO_2$ capture ratio (higher $CO_2$ volume fraction at the outlet) than expected with no evaporation. It has to be noted that for power plant capture systems, the flue gas treated by the HFMM is usually hydrated to some degree. Consequently, the evaporation of water from the liquid can be expected to be smaller than in the experimental system.

## 3.4 Ability to Predict Operation of Large Scale Modules

With the construction of large scale HFMM, the performance becomes harder to predict. The plastic grid, as shown in Figure 3b, is one example of the non-uniformities that can exist within the module which cause maldistribution of flows. Others include bends in the fibers, variations in the local fiber packing and varying thickness of the membranes. The ability to take into account these effects in a rigorous model is a challenge. Attempts have been made to capture the effects of non-uniformities, such as by considering a random distribution of fibers [37], however experiments at several different scales of HFMM are needed. The two orders of magnitude difference in size between the two HFMM considered here caused large differences in the ability to predict the operation. In order to understand how the non-uniformities evolve with each step increase in size and each variation in module construction, experimental data from many more systems are needed. This will then likely allow for correlations based on scale to be derived for the several parameters needed to accurately simulate HFMM operation.

## CONCLUSIONS

Two different scales of HFMM are constructed and operated to provide insight into the ability of predicting the behavior of HFMM at full scale. The results of the two-dimensional model based on mass and energy balances showed a good prediction of the performance of HFMM. For the lab-scale HFMM, with less non-ideality in the system, the model and experimental results fit very well for varying gas and liquid flow rates. When simulating the larger pilot-scale module, the prediction of the performance over a range of gas flow rates is not as good. The maldistribution of the flows around and inside the fibers is not accounted for in the 2D model and proved to be much more important in the pilot-scale module.

The assumption of uniform flow is one of the key assump-

tions used in the development of the model. Another is the hypothesis of a negligible evaporation of water. Although only modest temperature rises of up to 15°C are predicted by the simulations, this may have an effect in several ways. For one, the evaporation will cause a cooling effect in the liquid and decrease the temperature rise. This has implications for the diffusion of the compounds in the liquid, the density of both the gas and liquid and the reaction rates. Another effect of water in the gas phase is to decrease the partial pressure of $CO_2$. This will decrease the driving force for $CO_2$ to be absorbed into the liquid and thus decrease the capture ratio. It has not been possible to incorporate evaporation into the mass transfer model for this project, but this should clearly be a major focus of future work.

More generally, this contribution is one of the first attempts to experimentally evaluate the scale-up possibilities and limitations of membrane contactors from laboratory- to pilot-scale. Publications almost systematically refer to laboratory scale membrane contactors, while large scale applications (such as CCS) obviously require adequate simulation tools and extrapolation strategies for much larger units. This study has shown that the scale-up issue of membrane contactors is far from straightforward. Consequently, research and development efforts are urgently needed in this direction.

## REFERENCES

1 IPCC (2007) 4th Assessment Report (AR4), Climate Change 2007: Synthesis Report.

2 Energy-Related Carbon Dioxide Emissions, *International Energy Outlook 2010*, available at: http://www.eia.doe.gov/oiaf/ieo/emissions.html, accessed on 9 March 2012.

3 European Commission, Analysis of options to move beyond 20% greenhouse gas emission reductions and assessing the risk of carbon leakage, available on http://ec.europa.eu/clima/policies/package/index_en.htm, accessed on 9 March 2012.

4 Wang M., Lawal A., Stephenson P., Sidders J., Ramshaw C. (2010) Post-combustion $CO_2$ capture with chemical absorption: A state-of-the-art review, *Chem. Eng. Res. Design* **89**, 1609-1624.

5 Tobiesen F.A., Svendsen H.F., Juliussen O. (2007) Experimental Validation of a Rigorous Absorption Model for $CO_2$ postcombustion capture, *AIChE J.* **53**, 4, 846-865.

6 Abu-Zahra M.R.M., Schneiders L.H.J., Niederer J.P.M., Feron P.H.M., Versteeg G.F. (2007) $CO_2$ capture from power plants. Part I. A parametric study of the technical performance based on monoethanolamine, *Int. J. Greenhouse Gas Control* **1**, 37-46.

7 Gabelman A., Hwang S.T. (1999) Hollow fiber membrane contactors, *J. Membr. Sci.* **159**, 61-106.

8  Mansourizadeh A., Ismail A.F. (2009) Hollow fiber gas-liquid membrane contactors for acid gas capture: A review, *J. Hazardous Mater.* **17**, 38-53.

9  Mansourizadeh A., Ismail A.F., Matsuura T. (2010) Effect of operating conditions on the physical and chemical CO$_2$ absorption through the PVDF hollow fiber membrane contactor, *J. Membr. Sci.* **353**, 192-200.

10  Dindore V.Y., Brilman D.W.F., Versteeg G.F. (2005) Hollow fiber membrane contactor as a gas-liquid model contactor, *Chem. Eng. Sci.* **60**, 467-479.

11  Qi Z., Cussler E.L. (1985) Microporous Hollow fibers for gas absorption, *J. Membr. Sci.* **23**, 321-332.

12  Bottino A., Capannelli G., Comite A., Di Felice R., Firpo R. (2008) CO$_2$ removal from a gas stream by membrane contactor, *Sep. Purifi. Technol.* **59**, 85-90.

13  Lu J.G., Zheng Y.F., Cheng M.D., Wang L.J. (2007) Effects of activators on mass-transfer enhancement in a hollow fiber contactor using activated alkanolamine solutions, *J. Membr. Sci.* **289**, 138-149.

14  Mavroudi M., Kaldis S.P., Sakellaropoulos G.P. (2003) Reduction of CO$_2$ emissions by a membrane contacting process, *Fuel* **82**, 2153-2159.

15  Li J.L., Chen B.H. (2005) CO$_2$ absorption using chemicals solvents in hollow fiber membrane contactors, *Sep. Purifi. Technol.* **41**, 109-122.

16  Karoor S., Sirkar K.K. (1993) Gas absorption studies in microporous hollow fiber membranes modules, *Ind. Eng. Chem. Res.* **32**, 674-684.

17  Al-Marzouqi M., El-Naas M.H., Marzouk S.A.M., Al-Zarooni M.A., Abdullatif N., Faiz R. (2008) Modeling of CO$_2$ absorption in membrane contactors, *Sep. Purifi. Technol.* **59**, 286-293.

18  Lee Y., Noble R.D., Yeom B.Y., Park Y.I., Lee K.H. (2001) Analysis of CO$_2$ removal by hollow fiber membrane contactors, *J. Membr. Sci.* **194**, 57-67.

19  Wang R., Li D.F., Liang D.T. (2004) Modelling of CO$_2$ capture by three typical amine solutions in hollow fiber membrane contactors, *Chem. Eng. Process.* **43**, 849-856.

20  Boucif N., Favre E., Roizard D. (2008) CO$_2$ capture in HFMM contactor with typical amine solutions: A numerical analysis, *Chem. Eng. Sci.* **63**, 5375-5385.

21  Porcheron F., Drozdz S. (2009) Hollow fiber membrane contactor transient experiments for the characterization of gas/liquid thermodynamics and mass transfer properties, *Chem. Eng. Sci.* **64**, 265-275.

22  Shirazian S., Moghadassi A., Moradi S. (2009) Numerical simulation of mass transfer in gas-liquid hollow fiber membrane contactors for laminar flow conditions, *Simul. Modell. Pract. Theory* **17**, 708-718.

23  Zhang H.Y., Wang R., Liang D.T., Tay J.H. (2008) Theoretical and experimental studies of membrane wetting in the membrane gas-liquid contacting process for CO$_2$ absorption, *J. Membr. Sci.* **308**, 162-170.

24  Malek A., Teo W.K. (1997) Modeling of microporous hollow fiber membrane modules operated under partially wetted conditions, *Ind. Eng. Chem. Res.* **36**, 784-793.

25  Lu J.G., Zheng Y.F., Cheng M.D. (2008) Wetting mechanism in mass transfer process of hydrophobic membrane gas absorption, *J. Membr. Sci.* **308**, 180-190.

26  Faiz R., Al-Marzouqi M. (2009) Mathematical modeling for the simultaneous absorption of CO$_2$ and H$_2$S using MEA in hollow fiber membrane contactors, *J. Membr. Sci.* **342**, 269-278.

27  Boucif N., Favre E., Roizard D., Belloul M. (2008) Hollow fiber membrane contactor for hydrogen sulfide odor control, *AIChE J.* **54**, 122-131.

28  Nguyen P.T., Roizard D., Thomas D., Favre E. (2010) Gas permeability: A simple, novel and efficient method for testing membrane material/solvent compatibility for membrane contactors applications, *Desalination Water Treatment* **14**, 7-14.

29  Dindore V.Y., Brilman D.W.F., Feron P.H.M., Versteeg G.F. (2004) CO$_2$ absorption at elevated pressures using a hollow fiber membrane contactor, *J. Membr. Sci.* **235**, 99-109.

30  Chen S.C., Lin S.H., Wang Y.H., Hsiao H.C. (2011) Chemical absorption of carbon dioxide with asymmetrically heated polytetrafluoroethylene membranes, *J. Environ. Manage.* **92**, 1083-1090.

31  Takahashi N., Furuta Y., Fukunaga H., Takatsuka T., Mano H., Fujioka Y. (2011) Effects of membrane properties on CO$_2$ recovery performance in a gas absorption membrane contactor, *Energy Procedia* **4**, 693-698.

32  Hedayat M., Soltanieh M., Mousavi S.A. (2011) Simultaneous separation of H$_2$S and CO$_2$ from natural gas by hollow fiber membrane contactor using mixture of alkanolamines, *J. Membr. Sci.* **377**, 191-197.

33  Boributh S., Assabumrungrat S., Laosiripojana N., Jiraratananon R. (2011) A modelling study on the effects of membrane characteristics and operating parameters on physical absorption of CO$_2$ by hollow fiber membrane contactor, *J. Membr. Sci.* **380**, 21-33.

34  deMontigny D., Tontiwachwuthikul P., Chakma A. (2005) Using polypropylene and polytetrafluoroethylene membranes in a membrane contactor for CO$_2$ absorption, *J. Membr. Sci.* **277**, 99-107.

35  Nishikawa N., Ishibashi M., Ohta H., Akutsu N., Matsumoto H., Kamata T., Kitamura H. (1995) CO$_2$ removal by hollow fiber gas liquid contactor, *Energy Convers. Manage.* **36**, 415-418.

36  Khaisri S., deMontigny D., Tontiwachwuthikul P., Jiraratananon R. (2010) Comparing membrane resistance and absorption performance of three different membranes in a gas absorption membrane contactor, *Sep. Purifi. Technol.* **65**, 290-297.

37  Keshavarz P., Ayatollahi S., Fathikalajahi J. (2008) Mathematical modeling of gas-liquid membrane contactors using random distribution of fibers, *J. Membr. Sci.* **325**, 98-108.

38  Happel J. (1959) Viscous flow relative to arrays of cylinders, *AIChE J.* **5**, 174-177.

39  Blauwhoff P.M.M., Versteeg G.F., van Swaaij W.P.M. (1982) A study on the reaction between CO$_2$ and alkanolamines in aqueous solutions, *Chem. Eng. Sci.* **39**, 2, 207-225.